PCCP

PAPER

View Article Online
View Journal | View Issue

Cite this: *Phys. Chem. Chem. Phys.*, 2016, **18**, 13811

Investigation of the electrochemical and photoelectrochemical properties of Ni–Al LDH photocatalysts†

Shoji Iguchi,[a] Soichi Kikkawa,[a] Kentaro Teramura,*[abc] Saburo Hosokawa[ab] and Tsunehiro Tanaka*[ab]

Received 10th March 2016,
Accepted 16th April 2016

DOI: 10.1039/c6cp01646d

www.rsc.org/pccp

Layered double hydroxide (LDH) photocatalysts, including Ni–Al LDH, are active for the photocatalytic conversion of CO_2 in water under UV light irradiation. In this study, we found that a series of LDHs exhibited anodic photocurrent which is a characteristic feature corresponding to n-type materials. Also, we estimated the potentials of photogenerated electrons and holes for LDHs, which are responsible for the photocatalytic reactions, using electrochemical techniques. The flat band potential of the Ni–Al LDH photocatalyst was estimated to be −0.40 V *vs.* NHE (pH = 0), indicating that the potential of the photogenerated electron is sufficient to reduce CO_2 to CO. Moreover, we revealed that the flat band potentials of M^{2+}–M^{3+} LDH are clearly influenced by the type of trivalent metal (M^{3+}) components.

Introduction

Layered double hydroxides (LDHs), also known as anionic clays,[1–3] have the general formula $[M_{1-x}^{2+}\text{–}M_x^{3+}(OH)_2](A^{n-})_{x/n}\cdot mH_2O$, where M^{2+} and M^{3+} are divalent and trivalent cations, respectively; A^{n-} is an interlayer anion of valence n; and x denotes the molar ratio of $M^{3+}/(M^{2+} + M^{3+})$. The metal cations occupy the centers of edge-sharing octahedra, whose vertexes contain hydroxide ions that connect to form infinite two-dimensional sheets. Currently, many advanced applications for LDHs have been developed: for example, anion conductive materials,[4–7] capacitors,[8–11] electrocatalysts[12] and photocatalysts.[13–15] Some reactions carried out using these photocatalysts are photocatalytic degradation of organic compounds using a series of Zn-containing LDHs (Zn–Al, Zn–Bi, and Zn–Ti LDH)[14,16,17] and a CeO_2/Mg–Al LDH composite,[18] half-reactions of photocatalytic water splitting in the presence of sacrificial reagents using Ti-containing LDHs (Ni–Ti and Zn–Ti LDH)[19,20] and Zn–Cr LDH,[21] and photocatalytic conversion of CO_2.[22–25] We developed a photocatalytic system for the conversion of CO_2 in aqueous solution using Ni–Al LDH,[26,27] which enables the selective formation of CO (as the reduction product of CO_2) because of the complete suppression of H_2 evolution *via* the reduction of protons (H^+). The hydroxyl groups on the surface of LDH might act as an adsorption site for the dissolved CO_2 molecules in the reaction solution. In such a case, photoirradiation through Pyrex glass did not induce any photocatalytic reaction over Ni–Al LDH, whereas the use of quartz glass allowed the photocatalytic conversion of CO_2, indicating that UV light irradiation ($\lambda < 300$ nm) is necessary for this photocatalytic reaction.[28] In contrast, García *et al.* reported that Zn–Cr LDH was an active photocatalyst for the oxidation of H_2O into O_2 under visible light irradiation.[21] Because LDHs show photocatalytic activities for several kinds of reactions as reported by us and others (as cited above), there must be an energy gap that can induce photocatalytic reactions under illumination. However, only a few studies have investigated the electrochemical properties of these LDHs, such as energy gap measurement, charge separation induced by photoirradiation, and potentials of photogenerated electrons and holes. Concerning the reduction of CO_2 in aqueous media, the relationship between the standard potential for CO_2 (*i.e.*, $E^\circ(CO_2/CO) = -0.11$ V *vs.* NHE)[29] and the potential of the photoexcited electron in the photocatalyst material must be considered carefully because it is difficult to reduce CO_2, one of the most stable molecules, particularly in comparison with the reduction of a proton ($E^\circ(H^+/H_2) = 0.0$ V *vs.* NHE).[29]

Electrochemical and photoelectrochemical measurements are useful techniques that are widely used in the field of photocatalysis to understand the photocatalytic properties of materials, such as the distinction between n-type and p-type semiconductors, photon-to-current conversion efficiencies, energy levels of the

[a] *Department of Molecular Engineering, Graduate School of Engineering, Kyoto University, Kyotodaigaku Katsura, Nishikyo-ku, Kyoto 615-8510, Japan. E-mail: teramura@moleng.kyoto-u.ac.jp; Fax: +81-75-383-2561; Tel: +81-75-383-2559*
[b] *Elements Strategy Initiative for Catalysts & Batteries (ESICB), Kyoto University, 1-30 Goryo-Ohara, Nishikyo-ku, Kyoto 615-8245, Japan*
[c] *Precursory Research for Embryonic Science and Technology (PRESTO), Japan Science and Technology Agency (JST), 4-1-8 Honcho, Kawaguchi, Saitama 332-0012, Japan*

† Electronic supplementary information (ESI) available. See DOI: 10.1039/c6cp01646d

bottom of the conduction band (hereinafter "E_{CB}") and the top of the valence band (hereinafter "E_{VB}"), and the energy gap of the band structure (hereinafter "E_{BG}").[30] Electrochemical properties can be investigated by observing the interface between the semiconductor electrode and the electrolyte solution while applying an external bias to the former.[31,32] When a certain potential is applied, the Fermi level of the semiconductor lies at the same energy as the redox potential of the electrolyte solution, and there is no charge transfer between them; thus, no band bending occurs. This potential is referred to as the flat band potential (hereinafter "E_{FB}").[33,34] For n-type semiconductors,[31] the cathodic dark current is detected when the applied potential is more negative than E_{FB} because the accumulation layer, which appears under cathodic polarization, enables electron transfer from the electrode to the electrolyte solution, similar to that of a metallic electrode. In contrast, n-type semiconductors can act as photoanodes under anodic polarization. The photogenerated hole (h^+) in the depletion layer can move toward the interface, in accordance with band bending, and can easily receive electrons from the electrolyte solution. This permits electron transfer from the semiconductor to the counter electrode through a conductor cable, which is regarded as the anodic photocurrent. The values of E_{FB} and E_{BG} for semiconductor photocatalysts can be determined experimentally by using the Mott–Schottky and Davis–Mott equations; the details are presented in the Experimental section.

Recently, Wei *et al.* reported the theoretical studies on the band edge placement of M^{2+}–M^{3+} LDHs (M^{2+} = Mg^{2+}, Co^{2+}, Ni^{2+}, and Zn^{2+}; M^{3+} = Al^{3+} and Ga^{3+}), and the relationship between the band position and the photocatalytic activity for water oxidation was discussed.[35] In the present study, we have demonstrated properties such as the photoresponse character, energy gap, and potential of the photogenerated electron and hole for LDHs including Ni–Al LDH, which show the photocatalytic activities for the conversion of CO_2 in water, using experimental techniques based on photoelectrochemical considerations.

Experimental section

Electrode preparation

Ni–Al LDH was synthesized using a typical coprecipitation method. An aqueous solution containing $NiCl_2{\cdot}6H_2O$ (99.9%, Wako) and $AlCl_3$ (98.0%, Wako) was slowly dropped into an aqueous Na_2CO_3 (99.5%, Wako) solution at room temperature. The pH of the solution was kept stable between 9.9 and 10.1 by adding an aqueous NaOH (97.0%, Wako) solution using a liquid feed pump (NRP-76, NISSHIN RIKA). The resulting suspension was aged at 383 K under hydrothermal conditions using a stainless steel autoclave equipped with an inner Teflon vessel. The solid cake was collected by filtration and washed with ultra-pure water, and then dried at 383 K in air. Other combinations of metal components in LDH, such as Mg–Al, Zn–Al, Ni–Ga, and Ni–In, were fabricated *via* the same procedure as Ni–Al LDH using chloride salts as precursors.

For electrochemical and a photoelectrochemical measurements, LDH electrodes were prepared on a fluorine doped tin oxide (FTO) glass *via* an electrophoresis deposition method. 100 mg of LDH powder was added into 50 mL of an acetone solution containing 10 mg of iodine as an electrolyte, and then the LDH powder was dispersed thoroughly by ultrasonication. Prior to use, FTO glass (AGC fabritech Co., Ltd) was washed with acetone and 2-propanol solution in turn. Two FTO glasses were immersed in the solution facing each other, and direct current (DC) was applied between the two FTO glasses by using an electrochemical measurement system (HZ-5000, Hokuto Denko Corp.), at 0.1 mA stable current (2 min) for measurements in an aqueous solution, and at 10.0 V stable voltage (5 min) for those in an organic solution. After drying at room temperature in air, the prepared LDH electrode (hereinafter, called the X LDH/FTO electrode, X = Ni–Al, Mg–Al, Zn–Al, Ni–Ga, and Ni–In) was heated at 473 K for 2 h in order to remove the residual iodine. As reference electrodes, TiO_2/FTO and Ta_2O_5/FTO electrodes were prepared *via* the same procedure using TiO_2 (ST-01, Ishihara Sangyo Kaisha, Ltd) and Ta_2O_5 (Kojundo Chemical Laboratory Co., Ltd) as powder samples.

Characterization

X-ray diffraction (XRD) patterns of the prepared electrodes were collected by using an X-ray diffractometer (Multiflex, Rigaku) using Cu K_α radiation at an acceleration voltage of 40 kV with 0.02° per step. Scanning electron microscopy images for a sectioned view of the electrodes were captured by using a Field Emission Scanning Electron Microscope (SU-8220, Hitachi High-Technologies) at an acceleration voltage of 3.0 kV. UV/Vis diffuse reflectance spectra of LDH powder samples were measured using a UV-Visible spectrometer (V-670, JASCO) equipped with an integrated sphere accessory. The energy gap (hereinafter "E_g") of a series of LDHs and the E_{BG} of TiO_2 and Ta_2O_5 were determined by the Davis–Mott equation[36] using the Kubelka–Munk function $F(R_\infty)$ obtained from the diffuse reflectance spectrum,

$$[F(R_\infty)h\nu]^{-n} = A(h\nu - E_g) \quad (1)$$

where h, ν, and A are Planck's constant, frequency of vibration, and proportional constant, respectively.

Electrochemical measurements

Electrochemical measurements were performed using a three-electrode electrochemical cell consisting of the prepared LDH/FTO electrode, Ag/AgCl electrode, and Pt wire as the working electrode, reference electrode, and counter electrode, respectively. Prior to the measurements, the dissolved air in the electrolyte solution was completely removed by He gas flow. For a cyclic voltammetry, acetonitrile solution was used as a solvent, which contains 0.05 M of $LiClO_4$ as the electrolyte. The current value was recorded as the applied voltage was varied from −2.0 to 1.0 V *vs.* Ag/AgCl at a sweep rate of 10 mV s^{-1} using an electrochemical measurement system (HZ-5000, Hokuto Denko Corp.). For impedance measurements, an aqueous Na_2SO_4 solution (0.1 M) was used as an electrolyte solution. The imaginary component of the impedance (Z'') of the equivalent circuit including the X LDH/FTO electrode (X = Ni–Al, Mg–Al, Zn–Al, Ni–Ga, or Ni–In) was evaluated at an alternating current

frequency of 72.0, 52.0, and 37.3 kHz with a sweeping applied voltage from 0.5 to −0.5 V *vs.* Ag/AgCl using an electrochemical measurement system (HZ-5000, Hokuto Denko Corp.). The capacitance (C) of the circuit was calculated from the imaginary component of the impedance (Z'') using the relation,

$$|Z''| = 1/(2\pi fC) \quad (2)$$

where π and f denote the circumference ratio and the frequency of the alternating current. The value of E_{FB} for the working electrode was estimated by using the resulting value of C in accordance with the Mott–Schottky equation,

$$C^{-2} = (2/\varepsilon\varepsilon_0 A^2 e N_D)(E - E_{FB} - k_B T/e) \quad (3)$$

where C and A are the interfacial capacitance and area, respectively, N_D the number of donors, E the applied potential, k_B Boltzmann's constant, T the absolute temperature, ε the dielectric constant of the semiconductor, ε_0 the permittivity of free space, and e is the electronic charge. Therefore, the value of E_{FB} should be obtained from the intercept of the x-axis in the plot of C^{-2} *versus* the applied potential E. In the present study, the energy gap, the potential of the photogenerated electron and hole are hereinafter represented as E_g, E_e and E_h for a series of LDHs, and the band gap energy, the potential of the bottom of the conduction band and the top of the valence band are called as E_{BG}, E_{CB} and E_{VB} for TiO_2 and Ta_2O_5 typical semiconductor photocatalysts. The difference of potential (E) derived from the value of pH of the electrolyte solution was revised in accordance with the Nernst equation as below,

$$E_{(pH=a)} = E_{(pH=b)} - 0.059 \times (a - b) \quad (4)$$

where $E_{(pH=a)}$ and $E_{(pH=b)}$ are the values of potential at pH = a and b. For example, 0.00 V at pH = 0.0 should be converted into 0.41 V at pH = 7.0. Furthermore, the difference of potential with kinds of standard electrodes was converted to the normal hydrogen electrode (NHE) by using relationships as presented below for the silver–silver chloride standard electrode (Ag/AgCl)[37,38] and the standard calomel electrode (SCE).[37,38]

$$E(vs.\ \text{NHE}) - E(vs.\ \text{Ag/AgCl}) = 0.199\ \text{V} \quad (5)$$

$$E(vs.\ \text{NHE}) - E(vs.\ \text{SCE}) = 0.244\ \text{V} \quad (6)$$

Photoelectrochemical measurements

Photoelectrochemical measurements were conducted using a three-electrode electrochemical cell equipped with a quartz window. The prepared LDH/FTO electrode, the Ag/AgCl electrode, and Pt wire were used as the working electrode, reference electrode, and counter electrode, respectively. For the measurement in an organic solvent, $LiClO_4$ acetonitrile solution (0.05 M) containing 5 vol% methanol was used as the electrolyte solution. In contrast, an aqueous Na_2SO_4 solution which contains 5 vol% methanol was used for the measurement in an aqueous solution. In both cases, the solution was thoroughly degassed by He gas flow. The working electrode (X LDH/FTO, X = Ni–Al, Mg–Al, and Zn–Al) was irradiated using a 200 W Hg–Xe lamp (SAN-EI Electric Co., Ltd) through the quartz window. The photocurrent value was collected using an electrochemical measurement system (HZ-5000, Hokuto Denko Corp.) without an external bias. For linear sweep voltammetry under photoirradiation, the applied bias was swept from −1.5 to 1.0 V *vs.* Ag/AgCl.

Results and discussion

Fig. 1A shows the X-ray diffraction (XRD) pattern of the prepared Ni–Al LDH/FTO composite. Compared to those of the Ni–Al LDH powder sample (a) and bare FTO glass (c), the XRD pattern of Ni–Al LDH/FTO (b) shows mixed diffraction peaks of the above two samples. Two low angle peaks, 11° and 23°, in the powder sample are indexed as (0 0 3) and (0 0 6) planes, respectively, which define the characteristic layer structure of the LDH powders.[1] The peak positions of these reflections correspond to the layer-to-layer thickness; that is, the interlayer distance is equal to $d_{(0\,0\,3)}$ with respect to hexagonal axes. As shown in Fig. 1B, Ni–Al LDH/FTO exhibited small peaks around the same position as those in the powder sample, indicating that Ni–Al LDH is fixed onto the FTO glass and retains its layer structure. Moreover, the interlayer distance was conserved after the deposition onto FTO, because the positions of the (0 0 3) and (0 0 6) reflections were unchanged. As previously reported,[26,27] other LDHs (Mg–Al, Zn–Al, Ni–Ga, and Ni–In LDH) were successfully synthesized (XRD patterns of powder samples of these prepared LDHs are presented in Fig. S1, ESI†). Moreover, the specific surface area of the Ni–Al LDH powder sample was estimated to be *ca.* 100 $m^2\ g^{-1}$. Fig. 2A shows the SEM images of Ni–Al LDH/FTO prepared using the electrophoresis deposition method. Regions X and Y mark the deposited Ni–Al LDH region and the FTO glass, respectively. We found that Ni–Al LDH particles with a thickness of several micrometers were deposited on the FTO glass. Regarding the enlarged views shown in Fig. 2B, flower-petal-like morphologies, which are characteristic of LDH-type materials,[1,39] were also maintained. These SEM images are consistent with the results of XRD measurements of Ni–Al LDH/FTO. Based on the XRD patterns and SEM images, the state of the Ni–Al LDH deposited on FTO glass is considered to be similar to that of the powder sample, which shows photocatalytic activity for the conversion of CO_2 in aqueous solution.[26,28]

Fig. 3 shows the cyclic voltammogram recorded using a three-electrode electrochemical cell. The prepared Ni–Al LDH/FTO was used as the working electrode under a He atmosphere. When the working electrode was set under cathodic polarization, the cathodic dark current was determined, indicating that electron transfer from the working electrode to the electrolyte solution occurred because of the formation of an accumulation layer at the interface of the electrode, making the electron flow possible without an electric barrier. The cathodic dark current under cathodic polarization is known to be a characteristic feature of n-type semiconductor materials. In contrast, anodic current should not be found under dark conditions for n-type electrodes because of the band bending in the depletion layer. However, two anodic current peaks were found. Because the standard potential was reported as $E^\circ(IO_3^-/I^-) = 1.08$ V *vs.* NHE (pH = 0),[29]

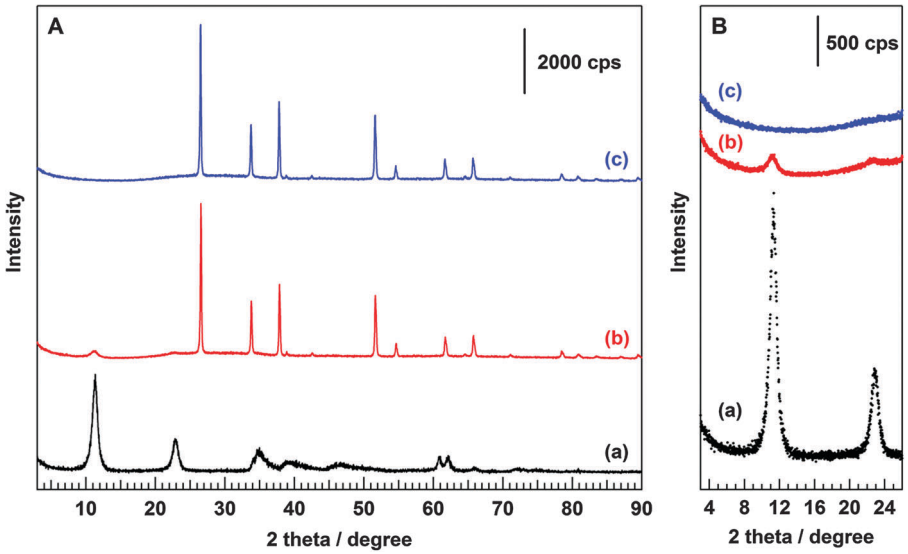

Fig. 1 XRD patterns of (a) Ni–Al LDH powder sample, (b) Ni–Al LDH/FTO, and (c) bare FTO collected in a (A) wide range scan and (B) narrow range scan.

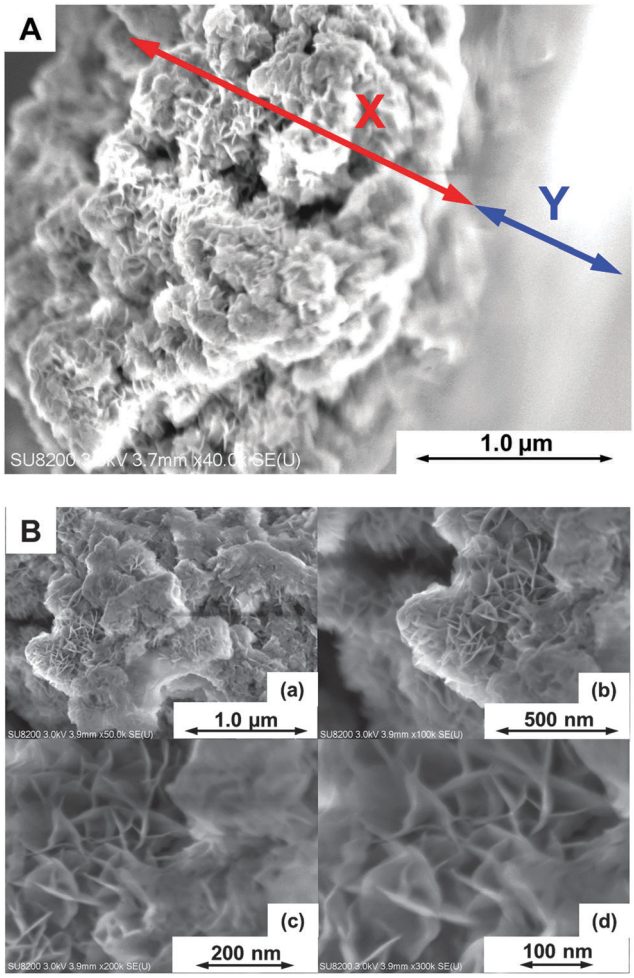

Fig. 2 Sectioned view of SEM images of Ni–Al LDH/FTO captured at a magnification of (A) 40.0k, (B-a) 50.0k, (B-b) 100k, (B-c) 200k, and (B-d) 300k. The regions X and Y in the image (A) indicate the deposited Ni–Al LDH layer and the FTO substrate, respectively.

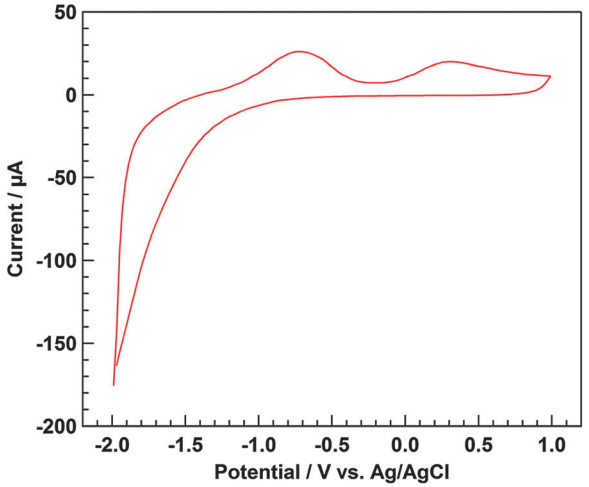

Fig. 3 Cyclic voltammogram of Ni–Al LDH/FTO. Electrochemical cell: Ni–Al LDH/FTO working electrode, Ag/AgCl reference electrode, Pt wire counter electrode, and 0.05 M $LiClO_4$ acetonitrile electrolyte solution. Atmosphere: He. Sweep range: from −2.0 to 1.0 V, and return to −2.0 V. Sweep rate: 10 mV s^{-1}.

the first peak, at *ca.* 0.4 V *vs.* Ag/AgCl, was assigned to the oxidation of I^- to IO_3^-, derived from I_2 that was used in the electrophoresis process. However, we were unable to assign the other peak, at *ca.* −0.2 V, to any reaction.

Fig. 4A shows the photocurrent values of the Ni–Al LDH/FTO working electrode under illumination cycling through the quartz window with no applied external bias. The anodic photocurrent increased upon illumination and diminished when the illumination stopped. The use of acetonitrile solution containing $LiClO_4$ resulted in a higher photocurrent than that compared to the use of an aqueous Na_2SO_4 solution. In both cases, the addition of methanol into the electrolyte solution was necessary to induce the anodic photocurrent, indicating that photogenerated holes (h^+)

can oxidize methanol in the electrolyte solution and photoexcited electrons (e^-) can transfer to the counter electrode as an anodic current. As shown in Fig. 4B, the substitution of Ni^{2+} in Ni–Al LDH by either Mg^{2+} or Zn^{2+} affected the photocurrent value, and the order of the initial photocurrent intensity was (e) Zn–Al LDH >, (d) Mg–Al LDH > and (c) Ni–Al LDH. This agrees with the quantity of electrons consumed in the photocatalytic conversion of CO_2 in water using these LDHs (powder samples) as previously shown;[26] specifically, the amount of electrons used to reduce CO_2 and H^+ (CO and H_2 were produced as reduction products) during 8 h of photoirradiation was 254, 110, and 68 μmol for Zn–Al LDH, Mg–Al LDH, and Ni–Al LDH, respectively (see the ESI† for the details of powder reaction: Table S1). Although Ni–Al LDH led to the evolution of the largest amount of CO and showed the highest selectivity among these M^{2+}–Al LDHs, the total amount of reduction products was largest in the Zn–Al LDH because, in that case, a large amount of H_2 was evolved. The photocurrent values measured in the present study are considered to reflect the total photocatalytic activities of the LDH photocatalysts; that is, the metal components of the hydroxide sheets alter the photocatalytic activity of a series of LDH materials, and Zn–Al LDH is a good photocatalyst based on the results of the photoelectrochemical measurements. Nevertheless the photocurrent value was smaller than others; Ni–Al LDH can reduce CO_2 into CO with high selectivity (Table S1, ESI†). However, it is possible that self-oxidation of Zn–Al LDH by the photogenerated holes led to a rapid decrease in the photocurrent intensity, as reported for the case of ZnO.[40] Fig. 4C shows the photocurrent value of Ni–Al LDH/FTO under cycled illumination in a photoelectrochemical cell using an aqueous Na_2SO_4 solution as the electrolyte. In regions (f) and (k), photoirradiation was performed using a Hg–Xe lamp through a quartz window. For regions (g), (h), (i), and (j), long-pass cut-off filters UV-29, UV-31, UV-33, and UV-35, respectively, were set to control the photoirradiation wavelengths. The photocurrent intensity under photoirradiation through the UV-29 filter was much smaller than that through the quartz window. Moreover, the use of UV-31, UV-33, or UV-35 significantly diminished the photocurrent value during illumination. This result indicates that UV light irradiation of <270 nm is necessary to induce photocatalytic reactions over Ni–Al LDH, because a very low percentage of light at 270 nm can be transmitted through the UV-29 filter. Based on a Davis–Mott plot of Ni–Al LDH shown in Fig. S2 (ESI†), the band gap energy of Ni–Al LDH is estimated at 4.8 eV (=258 nm). This value is consistent with the results of the wavelength dependence measurements on the photocurrent intensity.

Fig. 5 shows the linear sweep voltammograms measured while the light source was cycled on and off under a He atmosphere. Under anodic polarization, the anodic photocurrent flowed when photoirradiation started. The presence of a depletion layer at the interface of the electrode under anodic polarization enables the separation of the photogenerated charge carriers. Accordingly, for an n-type material at the positive potential, the band edges curve upwards, the hole moves toward the interface, and the electron moves to the interior of the material.[31,32] Holes are high-energy

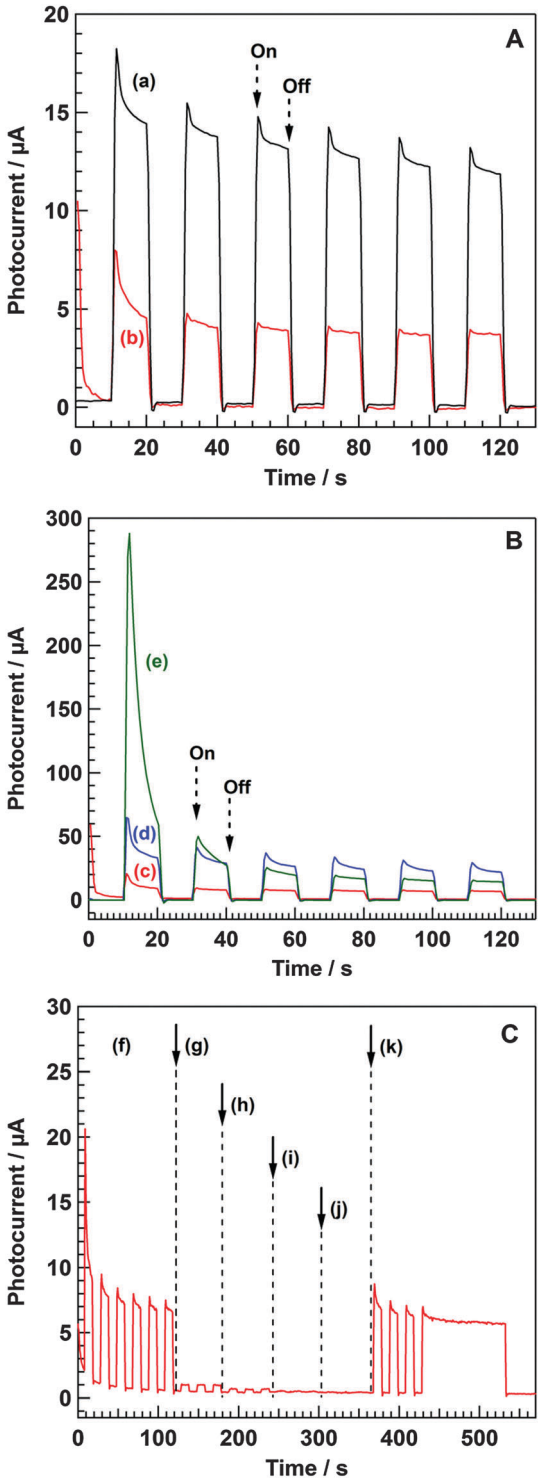

Fig. 4 Photocurrent intensity with the repetition of turning on and off the illumination for X LDH/FTO (X = Ni–Al, Mg–Al, and Zn–Al). (A) Ni–Al LDH/FTO measured in (a) 0.05 M $LiClO_4$ acetonitrile (5 vol% methanol) and (b) 0.1 M Na_2SO_4 aq. (5 vol% methanol). (B) (c) Ni–Al LDH/FTO, (d) Mg–Al LDH/FTO, and (e) Zn–Al LDH/FTO measured in 0.05 M $LiClO_4$ acetonitrile (5 vol% methanol). (C) Ni–Al LDH/FTO measured in 0.05 M $LiClO_4$ acetonitrile (5 vol% methanol) under the photoirradiation through (f) quartz glass, (g) UV-29, (h) UV-31, (i) UV-33, (j) UV-35, and (k) quartz glass. Electrochemical cell: X LDH/FTO (X = Ni–Al, Mg–Al, and Zn–Al) working electrode, Ag/AgCl reference electrode, and Pt wire counter electrode. Atmosphere: He.

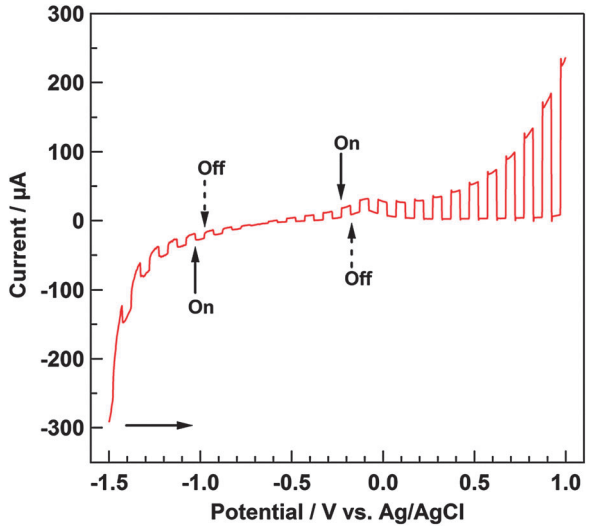

Fig. 5 Linear sweep voltammogram of Ni–Al LDH/FTO measured with the repetition of turning on and off the illumination. Electrochemical cell: Ni–Al LDH/FTO working electrode, Ag/AgCl reference electrode, Pt wire counter electrode, and 0.05 M $LiClO_4$ acetonitrile (5 vol% methanol) electrolyte solution. Atmosphere: He. Sweep range: from −1.5 to 1.0 V. Sweep rate: 10 mV s^{-1}. Photoirradiation: through quartz glass window.

species that can extract an electron from the electrolyte solution; that is, the n-type material acts as a photoanode under anodic polarization. Based on this, it can be inferred that Ni–Al LDH has electrochemical properties corresponding to an n-type material. In contrast, a small cathodic photocurrent was observed under cathodic polarization, which generally results from the p-type character. We presumed that the cathodic photocurrent was due to the self-reduction of Ni species in Ni–Al LDH: from Ni^{2+} to Ni^0 ($E^\circ(Ni^{2+}/Ni) = -0.26$ V *vs.* NHE (pH = 0))[29] or from NiOOH to $Ni(OH)_2$ ($E^\circ(NiOOH/Ni(OH)_2) = 0.52$ V *vs.* NHE (pH = 0)),[29] because it can be estimated that Ni^{2+} incoporated into Ni–Al LDH was oxidized by the anodic applied potential during the electrophoresis method. Therefore, Mg–Al LDH did not show the cathodic photocurrent at that region. Moreover, the onset potential for the anodic photocurrent, based on the shape of the photocurrent profile during photoirradiation cycling, was estimated to be *ca.* −0.75 V *vs.* Ag/AgCl in this study.

Fig. 6A–C show the Mott–Schottky plots of X LDH/FTO (X = Ni–Al, Mg–Al, Zn–Al, Ni–Ga, and Ni–In), TiO_2/FTO, and Ta_2O_5/FTO based on the impedance measurements using these materials as working electrodes. As mentioned above, the flat band potential (E_{FB}) can be determined by extrapolation to $C^{-2} = 0$ (C: capacitance), in accordance with the Mott–Schottky equation. When impedance measurements are conducted at variable frequencies, the fitted line for each Mott–Schottky plot should converge at E_{FB} ($C^{-2} = 0$). In the case of Ni–Al LDH/FTO, the fitting lines of the Mott–Schottky plots for frequencies of 37.3, 52.0, and 72.0 kHz crossed at a point shifted from the *x*-axis intercept, as shown in Fig. 6A. Despite that, the E_{FB} of Ni–Al LDH/FTO was estimated to range from −0.9 to −0.7 V *vs.* NHE (pH = 6.2). Moreover, the incline of the fitting line for the Mott–Schottky plot was positive (rightward inclining), indicating that the Ni–Al LDH shows n-type semiconductor-like properties,[31] as we determined before from the photoelectrochemical measurements. Fig. 6B displays the Mott–Schottky plots of (d) TiO_2/FTO, (e) Ni–Al LDH/FTO, and (f) Ta_2O_5/FTO, recorded using an aqueous Na_2SO_4 solution (pH = 6.2) as an electrolyte under 52.0 kHz of the alternating current frequency. From this result, the E_{FB} of anatase TiO_2 was considered to be −0.55 V *vs.* NHE, and the value of E_{FB} matched with those of previous reports that described the energy position of the flat band for anatase TiO_2.[41,42] Similarly, the estimated value of E_{FB} of Ta_2O_5 in this study was −0.92 V *vs.* NHE (pH = 6.2), similar to those reported in the

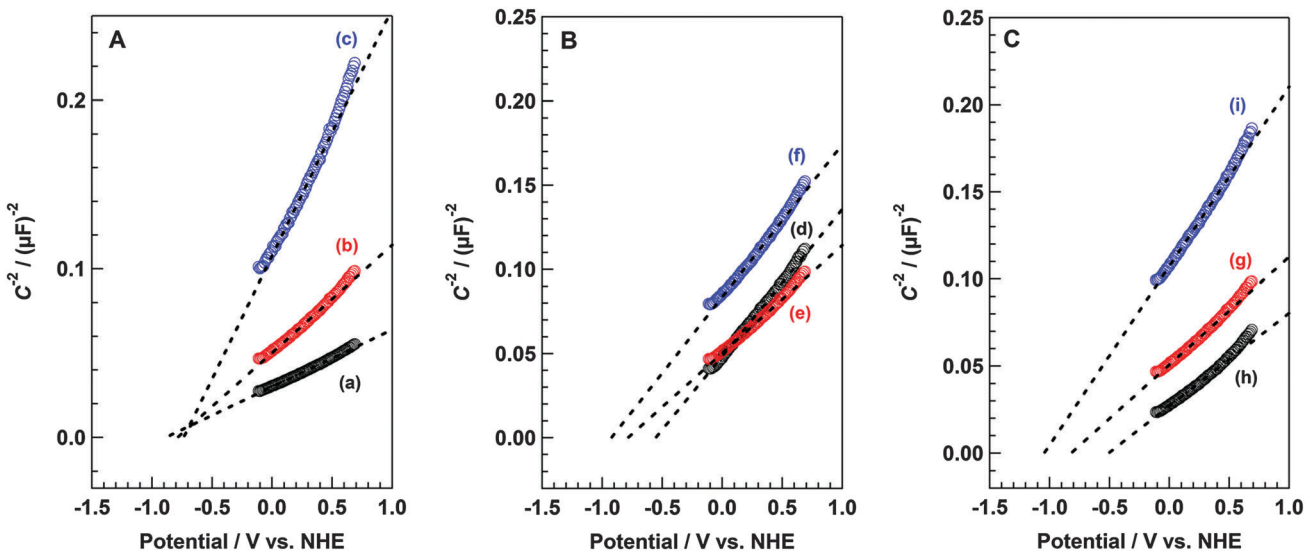

Fig. 6 Mott–Schottky plots based on the results of the impedance measurements. (A) Plots for Ni–Al LDH/FTO at a frequency of (a) 37.3, (b) 52.0, and (c) 72.0 kHz. (B) Plots for (d) TiO_2/FTO, (e) Ni–Al LDH/FTO, and (f) Ta_2O_5/FTO at a frequency of 52.0 kHz. (C) Plots for (g) Ni–Al LDH/FTO, (h) Ni–Ga LDH/FTO, and (i) Ni–In LDH/FTO at a frequency of 52.0 kHz. Electrochemical cell: X LDH/FTO (X = Ni–Al, Mg–Al, Zn–Al, Ni–Ga, and Ni–In), TiO_2/FTO, or Ta_2O_5/FTO working electrode, Ag/AgCl reference electrode, Pt wire counter electrode, and 0.1 M Na_2SO_4 aq. electrolyte solution. Atmosphere: He.

previous literature.[43] Compared to these reference samples, the position of E_{FB} in Ni–Al LDH was between those of TiO_2 and Ta_2O_5, and was determined to be −0.77 V *vs.* NHE (pH = 6.2). This value was slightly shifted from the onset potential obtained from the photocurrent observation by sweeping the applied bias (Fig. 5). Bolts *et al.* and Sprunken *et al.* have pointed out the dependence of the onset potential of photocurrent on experimental conditions such as surface coverage with reducible adsorbates, illumination intensity, wavelength, and pH of the electrolyte solution.[44,45] Concerning the present study, the results of the impedance measurements in accordance with the Mott–Schottky equation were used to determine the value of E_{FB}. Generally, the difference in the value of E_{FB} for n-type metal oxide semiconductors is considered to be due to the metal components, which form the conduction band. The conduction band of TiO_2 and Ta_2O_5 mainly comprise the Ti 3d and Ta 5d orbitals, respectively. As shown in Fig. 6C, a change in the estimated E_{FB} value was found upon the substitution of metal species of hydroxide sheets within the LDH structure. The incorporation of Ga^{3+} or In^{3+} instead of Al^{3+} into the Ni–Al LDH for the formation of Ni–Ga LDH or Ni–In LDH clearly influenced the value of E_{FB}, whereas the substitution of Ni^{2+} with Mg^{2+} or Zn^{2+} did not affect the value of E_{FB}, as shown in Fig. S3 (ESI†). Based on these results, we conclude that the potential of the photogenerated electrons for a series of M^{2+}–M^{3+} LDH group materials are regulated by M^{3+} species within the hydroxide sheets, rather than M^{2+} species. Moreover, the Mott–Schottky plot for Ni–Al LDH shifted to negative potential with increasing pH of the electrolyte solution in accordance with the Nernst equation (eqn (4)), as shown in Fig. S4 (ESI†).

Fig. 7 summarizes the results of the investigation of the electrochemical properties for X LDHs (X = Ni–Al, Mg–Al, Zn–Al, Ni–Ga, and Ni–In) and reference samples (TiO_2 and Ta_2O_5). Unless otherwise noted, the units of potential in this paragraph are quoted *vs.* NHE (pH = 0). Because the Fermi level for electrons of n-type character materials is considered to merge with the lowest potential of the conduction band,[30] the value of E_{FB} obtained through the impedance measurements in this study is read as that of E_e for the LDH photocatalysts, and that of E_{CB} for the TiO_2 and Ta_2O_5 typical semiconductor photocatalysts. The value of energy gap (E_g) between E_e and E_h for a series of LDHs, and the band gap (E_{BG}) between E_{CB} and E_{VB} for TiO_2 and Ta_2O_5 were estimated from UV/vis diffuse reflectance spectra based on the Davis–Mott plot, as shown in Fig. S2 (ESI†). In addition, the potential of the top of the valence band (E_{VB}) was calculated using the values of E_{CB} and E_{BG}. For the case of TiO_2, E_{CB} and E_{BG} were estimated to be −0.19 eV and 3.4 eV, respectively. The value of E_{CB} was adapted to that previously reported because −0.40 V *vs.* SCE (pH = 0) in the literature presented by Grätzel *et al.*[42] must be converted to −0.16 V *vs.* NHE (pH = 0) in accordance with eqn (6). The E_{BG} value determined in this study was slightly larger than the general value. For Ta_2O_5, the estimated values of E_{CB} and E_{VB} were, respectively, −0.56 V and 3.46 V, which are consistent with the results of electrochemical measurements in the literature reported by Domen and co-authors.[43] Based on these results for the reference samples, we suggest that the electrochemical character of X LDH (X = Ni–Al, Mg–Al, Zn–Al, Ni–Ga, and Ni–In) photocatalysts is as follows. For Ni–Al LDH, which has been reported as a photocatalyst for the selective conversion of CO_2 into CO in our previous studies,[26,28] E_e was −0.40 V, thereby satisfying the required potential for the reduction of CO_2 to CO; however, it was not enough for the one-electron reduction of CO_2 ($E^\circ(CO_2/CO_2^{\bullet-}) \approx -2.0$ V *vs.* NHE).[46] From this result, it can be inferred that the Ni–Al LDH photocatalyst might reduce CO_2 into CO in a two-electron process. On the other hand, E_h of Ni–Al LDH was found to be 4.39 V, significantly more positive than the value of E_{VB} for typical oxides such as TiO_2 and Ta_2O_5. Our experimental results for electrochemical properties of LDH photocatalysts were not fully consistent with the results of the theoretical studies.[35] As is often the case, the disagreement between experimental and theoretical results caused by the differences in limitations of the two

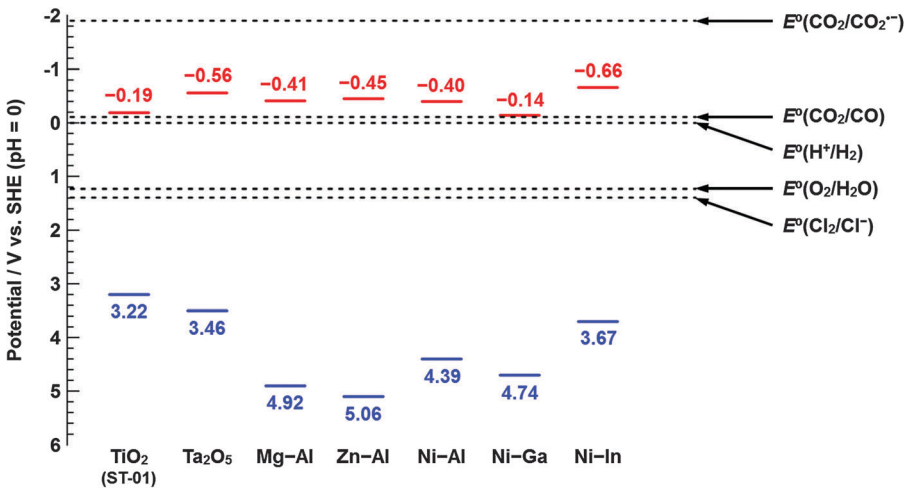

Fig. 7 Summary of the investigation of the electrochemical properties of X LDHs (X = Ni–Al, Mg–Al, Zn–Al, Ni–Ga, and Ni–In), and references (TiO_2 and Ta_2O_5). Standard potentials of redox couples are cited from the literature.[29,45] Potentials of the photogenerated electron and hole are, respectively, presented in red and blue color.

approaches should be considered in the near future. However, this potential is sufficient to oxidize Cl^- into Cl_2, as shown in Fig. 7 ($E^\circ(Cl_2/Cl^-) = 1.39$ V).[29] We previously insisted that Cl^- in the reaction solution can act as an effective hole scavenger for the photocatalytic conversion of CO_2 in an aqueous solution and Cl^- should be oxidized into Cl_2, which is immediately converted into hypochlorous acid (HClO).[28] By carrying out electrochemical investigations, we inferred that photogenerated electrons and holes in Ni–Al LDH are capable of reducing CO_2 into CO and oxidizing Cl^- into Cl_2. The changes in the value of E_h were determined by substituting Ni^{2+} in Ni–Al LDH with Mg^{2+} or Zn^{2+}, whereas the position of E_e was not influenced by the type of divalent metal (M^{2+}) in M^{2+}–Al LDH, as mentioned above. In contrast, the change of trivalent metal clearly affected the position of E_e; for example, the incorporation of In^{3+} shifted to a negative value compared to Al^{3+}, while the E_e of Ni–Ga LDH was found to have a positive potential, similar to the value of E_{CB} for TiO_2. By considering thermodynamic aspects, the reduction of protons to H_2 ($E^\circ(H^+/H_2) = 0.0$ V),[29] which competitively takes place in the photocatalytic conversion of CO_2 in an aqueous media, is relatively favorable in comparison to the reduction of CO_2 into CO ($E^\circ(CO_2/CO) = -0.11$ V)[29,46] because of their reduction potentials. The overpotential of the photoexcited electron toward the reduction of CO_2 into CO (ΔE_{OP}) is presented in accordance with eqn (7), as shown below.

$$\Delta E_{OP} = E^\circ(CO_2/CO) - E_e \quad (7)$$

where $E^\circ(CO_2/CO)$ and E_e are the standard potential of CO_2 reduction to CO and the potential of the photogenerated electron, estimated from E_{FB}, respectively. Hence, Ni–In LDH, whose photoexcited electron has a large overpotential in the reduction of CO_2 into CO ($\Delta E_{OP} = 0.55$ V) should be more advantageous for the selective reduction of CO_2 than Ni–Al LDH ($\Delta E_{OP} = 0.29$ V). However, the results of the photocatalytic conversion of CO_2 in water using powder samples indicated that Ni–Al LDH, whose E_e is more positive than that of Ni–In LDH, shows a higher selectivity toward CO_2 reduction among the reduction products (65.7% of the selectivity toward CO_2 reduction among the total reduction products; CO and H_2) rather than Ni–In LDH (less than 5%). In such a case, Ni–In LDH evolved large amounts of H_2 as the reduction product of H^+, indicating that the photogenerated electrons were mainly consumed in the reduction of H^+. In other words, Ni–Al LDH enabled the selective conversion of CO_2 in spite of its relatively positive E_e. This correlation clearly indicates that the selectivity toward CO_2 reduction and the inhibition of proton reduction to H_2 were determined by not only the overpotential of photogenerated electron but also the chemical properties and morphologies. Herein, we have clarified the photocurrent character and electrochemical properties such as potentials of photogenerated electrons and holes for a series of LDHs, including Ni–Al LDH, through electrochemical and photoelectrochemical measurements.

Conclusion

A series of LDHs (Ni–Al, Mg–Al, and Zn–Al LDH) were found to produce anodic photocurrent under no external bias, and the order of the initial photocurrent intensities were in accordance with the amount of electrons consumed in the photocatalytic conversion of CO_2 in water using these LDH powder samples. Ni–Al LDH had electrochemical properties corresponding to n-type materials; that is, a cathodic dark current under cathodic polarization and an anodic photocurrent under anodic polarization were determined by electrochemical measurements. The value of E_e for the Ni–Al LDH photocatalyst was estimated to be -0.40 V *vs.* NHE (pH = 0), which is enough to induce the two-electron reduction of CO_2 into CO. The change of M^{3+} metal in Ni–M^{3+} LDH clearly influenced E_e; E_e changed from negative to positive in the following order: Ni–In LDH, Ni–Al LDH, and Ni–Ga LDH. We concluded that the selectivity toward CO_2 reduction and the inhibition of proton reduction to H_2 are regulated not only by the overpotential of photogenerated electrons but also by the chemical properties of LDH photocatalysts.

Abbreviations

NHE	Normal hydrogen electrode
Ag/AgCl	Silver–silver chloride electrode
SCE	Standard calomel electrode
E_{CB}	Bottom of the conduction band for semiconductors
E_{VB}	Top of the valence band for semiconductors
E_{BG}	Energy gap of the band structure for semiconductors
E_{FB}	Flat band potential
E_e	Potential of the photogenerated electron for a series of LDHs
E_h	Potential of the photogenerated hole for a series of LDHs
E_g	Energy gap for a series of LDHs
Z''	Imaginary component of the impedance
C	Capacitance
π	Circumference ratio
f	Frequency of the alternating current
A	Area of the electrode
N_D	Number of carriers
E	Applied potential
k_B	Boltzmann's constant
T	Absolute temperature
ε	Dielectric constant
ε_0	Permittivity of free space
e	Electronic charge

Acknowledgements

This study was partially supported by a Grant-in-Aid for Scientific Research on Innovative Areas "All Nippon Artificial Photosynthesis Project for Living Earth" (No. 2406) of the Ministry of Education, Culture, Sports, Science, and Technology (MEXT) of Japan, the Precursory Research for Embryonic Science and Technology (PRESTO), supported by the Japan Science and Technology Agency (JST), and the Program for Elements Strategy Initiative for Catalysts & Batteries (ESICB), commissioned by the MEXT of Japan. Shoji Iguchi thanks the JSPS Research Fellowships for Young Scientists.

References

1 F. Cavani, F. Trifirò and A. Vaccari, *Catal. Today*, 1991, **11**, 173–301.
2 C. Delhoyo, *Appl. Clay Sci.*, 2007, **36**, 103–121.
3 B. F. Sels, D. E. De Vos and P. A. Jacobs, *Catal. Rev.*, 2001, **43**, 443–488.
4 Y. Arishige, D. Kubo, K. Tadanaga, A. Hayashi and M. Tatsumisago, *Solid State Ionics*, 2014, **262**, 238–240.
5 D. Kubo, K. Tadanaga, A. Hayashi and M. Tatsumisago, *J. Electroanal. Chem.*, 2012, **671**, 102–105.
6 D. Kubo, K. Tadanaga, A. Hayashi and M. Tatsumisago, *J. Power Sources*, 2013, **222**, 493–497.
7 K. Tadanaga, Y. Furukawa, A. Hayashi and M. Tatsumisago, *J. Electrochem. Soc.*, 2012, **159**, B368–B370.
8 J. Fang, M. Li, Q. Li, W. Zhang, Q. Shou, F. Liu, X. Zhang and J. Cheng, *Electrochim. Acta*, 2012, **85**, 248–255.
9 Z. Gao, J. Wang, Z. Li, W. Yang, B. Wang, M. Hou, Y. He, Q. Liu, T. Mann, P. Yang, M. Zhang and L. Liu, *Chem. Mater.*, 2011, **23**, 3509–3516.
10 A. Malak-Polaczyk, C. Vix-Guterl and E. Frackowiak, *Energy Fuels*, 2010, **24**, 3346–3351.
11 T. Stimpfling and F. Leroux, *Chem. Mater.*, 2010, **22**, 974–987.
12 D. H. Youn, Y. B. Park, J. Y. Kim, G. Magesh, Y. J. Jang and J. S. Lee, *J. Power Sources*, 2015, **294**, 437–443.
13 W. He, R. Wang, L. Zhang, J. Zhu, X. Xiang and F. Li, *J. Mater. Chem. A*, 2015, **3**, 17977–17982.
14 L. Mohapatra and K. M. Parida, *Phys. Chem. Chem. Phys.*, 2014, **16**, 16985–16996.
15 L. Wang, F. Dionigi, N. T. Nguyen, R. Kirchgeorg, M. Gliech, S. Grigorescu, P. Strasser and P. Schmuki, *Chem. Mater.*, 2015, **27**, 2360–2366.
16 M. Shao, J. Han, M. Wei, D. G. Evans and X. Duan, *Chem. Eng. J.*, 2011, **168**, 519–524.
17 S. J. Xia, F. X. Liu, Z. M. Ni, J. L. Xue and P. P. Qian, *J. Colloid Interface Sci.*, 2013, **405**, 195–200.
18 J. S. Valente, F. Tzompantzi and J. Prince, *Appl. Catal., B*, 2011, **102**, 276–285.
19 B. Li, Y. Zhao, S. Zhang, W. Gao and M. Wei, *ACS Appl. Mater. Interfaces*, 2013, **5**, 10233–10239.
20 Y. Zhao, P. Chen, B. Zhang, D. S. Su, S. Zhang, L. Tian, J. Lu, Z. Li, X. Cao, B. Wang, M. Wei, D. G. Evans and X. Duan, *Chemistry*, 2012, **18**, 11949–11958.
21 C. G. Silva, Y. Bouizi, V. Fornés and H. García, *J. Am. Chem. Soc.*, 2009, **131**, 13833–13839.
22 N. Ahmed, Y. Shibata, T. Taniguchi and Y. Izumi, *J. Catal.*, 2011, **279**, 123–135.
23 K.-I. Katsumata, K. Sakai, K. Ikeda, G. Carja, N. Matsushita and K. Okada, *Mater. Lett.*, 2013, **107**, 138–140.
24 M. Morikawa, N. Ahmed, Y. Yoshida and Y. Izumi, *Appl. Catal., B*, 2014, **144**, 561–569.
25 M. Morikawa, Y. Ogura, N. Ahmed, S. Kawamura, G. Mikami, S. Okamoto and Y. Izumi, *Catal. Sci. Technol.*, 2014, **4**, 1644–1651.
26 S. Iguchi, K. Teramura, S. Hosokawa and T. Tanaka, *Catal. Today*, 2015, **251**, 140–144.
27 K. Teramura, S. Iguchi, Y. Mizuno, T. Shishido and T. Tanaka, *Angew. Chem., Int. Ed.*, 2012, **51**, 8008–8011.
28 S. Iguchi, K. Teramura, S. Hosokawa and T. Tanaka, *Phys. Chem. Chem. Phys.*, 2015, **17**, 17995–18003.
29 *Standard Potentials in Aqueous Solution*, ed. A. J. Bard, R. Parsons and J. Jordan, Marcel Dekker, 1985.
30 R. Beranek, *Adv. Phys. Chem.*, 2011, **2011**, 1–20.
31 A. W. Bott, *Curr. Sep.*, 1998, **17**, 87–91.
32 L. L. K. Gelderman and S. W. Donne, *J. Chem. Educ.*, 2007, **84**, 685–688.
33 W. G. F. Cardon, *J. Phys. D: Appl. Phys.*, 1978, **11**, L63–L67.
34 W. J. Albery, G. J. O'Shea and A. L. Smith, *J. Chem. Soc., Faraday Trans.*, 1996, **92**, 4083–4085.
35 S.-M. Xu, T. Pan, Y.-B. Dou, H. Yan, S.-T. Zhang, F.-Y. Ning, W.-Y. Shi and M. Wei, *J. Phys. Chem. C*, 2015, **119**, 18823–18834.
36 E. A. Davis and N. F. Mott, *Philos. Mag.*, 1970, **22**, 0903–0922.
37 R. G. Bates, *Determination of pH: theory and practice*, John Wiley & Sons, 1973.
38 D. T. Sawyer, A. Sobkowiak and J. L. Roberts, *Electrochemistry for Chemists*, Wiley, 1995.
39 J. Zhang, X. Xie, C. Li, H. Wang and L. Wang, *RSC Adv.*, 2015, **5**, 29757–29765.
40 L. N. Elaziouti and B. Ahmed, *J. Chem. Eng. Process Technol.*, 2011, **2**, 106.
41 L. Kavan, M. Grätzel, S. E. Gilbert, C. Klemenz and H. J. Scheel, *J. Am. Chem. Soc.*, 1996, **118**, 6716–6723.
42 G. Rothenberger, D. Fitzmaurice and M. Grätzel, *J. Phys. Chem.*, 1992, **96**, 5983–5986.
43 W.-J. Chun, A. Ishikawa, H. Fujisawa, T. Takata, J. N. Kondo, M. Hara, M. Kawai, Y. Matsumoto and K. Domen, *J. Phys. Chem. B*, 2003, **107**, 1798–1803.
44 J. M. Bolts and M. S. Wrighton, *J. Phys. Chem.*, 1976, **80**, 2641–2645.
45 H. R. Sprunken, R. Schumacher and R. N. Schindler, *Faraday Discuss. Chem. Soc.*, 1980, **70**, 55–66.
46 J.-M. Lehn and R. Ziessel, *Proc. Natl. Acad. Sci. U. S. A.*, 1982, **79**, 701–704.